Magnetometer Bias Calibration Based on Relative Angular Position: Theory and Experimental Comparative Evaluation

Giancarlo Troni and Ryan M. Eustice

***Abstract*— This paper reports on a novel method for estimating the sensor bias of three-axis magnetometers (or any other field sensor). Our approach employs relative angular position measurements to estimate the three-axis magnetometer measurement bias, significantly improving magnetometer-based attitude estimation. Relative angular position measurements can be calculated from a variety of sources, including multiview image registration or laser-based scan matching. We report two methods implementing this approach based on batch linear least squares and a real-time discrete Kalman filter. Compared with previously reported methods our approach is time independent and less restrictive with data sampling. In addition, our two methods (*i*) are empirically shown to impose less restrictive conditions for the movements of the instrument required for calibration, (*ii*) do not require knowledge of the direction of the field (e.g., the local magnetic field) or the attitude of the instrument, and (*iii*) also ensure convergence for the estimated parameters. The proposed methods are evaluated and compared with previously reported methods in both numerical simulation and in comparative experimental evaluation using cameras and magnetometer sensors under different conditions.**

I. Introduction

Magnetometers and visual sensors are widely used in many applications including ground, space, air, and marine vehicle navigation systems. Magnetometers are commonly used to measure Earth's local magnetic field vector and thus determine the device heading (e.g., a digital compass). Magnetometers are highly affected by magnetic field disturbances that can cause bias, scale, and lack of orthogonality in the measured signals. Our approach employs relative rotation measurements estimated from visual sensors to estimate the bias of a three-axis magnetometer. The relative rotation measurements are commonly available from stereo or monocular visual odometry (VO) navigation systems (e.g., [20]), but the proposed approach can be used in combination with any method measuring the relative motion (e.g., laser-based scan-matching), as depicted in Fig.1. Two methods are proposed here based on this novel approach: (*i*) linear least squares and (*ii*) Kalman filtering. Our main motivation is for the problem of determining magnetometer sensor bias, but it can also be applied to any other field sensor such as three-axis accelerometers. The proposed solution does not, at present, include the estimation of scale and orthogonality factors, but it can be extended to these cases.

Several approaches for magnetometer calibration have been reported that estimate the calibration parameters without the use of additional reference sensors. The problem of self-calibrating a three-axis magnetometer without external reference can be formulated as a minimization problem that requires iterative methods to solve for the calibration parameters. For estimating magnetometer bias, Gambhir [7] proposed a "centered" approximation that can be solved with linear least squares. Alonso and Shuster proposed the "TWOSTEP" method, which uses Gambhir's solution as initialization to an iterative second step for estimating the sensor bias [3], and, as reported in a later work, also estimates the scale and orthogonality factors [2]. In a similar approach, Vasconcelos et al. [27] formulate the problem as an ellipsoid fitting problem, and solve it using an iterative maximum likelihood estimate (MLE) method. A closed-form solution to align the sensor is also proposed. Several limitations exist, however, for practical implementation in different applications. In general, all of these calibration methods require large angular movements of the instrument to measure a large section of the magnetic sensor output for an accurate calibration. For better performance it is necessary to know accurately the local magnitude of the Earth's magnetic field. This value can be calculated by magnetic field models, (e.g., [16]), but can present large error in environments with unmodeled magnetic distortions (e.g., due to buildings or other local magnetic anomalies). Finally, these methods are formulated for batch estimation and are not practical for continuous real-time operation.

Some previously reported methods for calibrating magnetometers use additional sensors to estimate the measurement bias. The requirement of additional sensors limit their use but it allows to overcome some of the limitation of magnetometer-only calibration methods. Li and Li [13] and

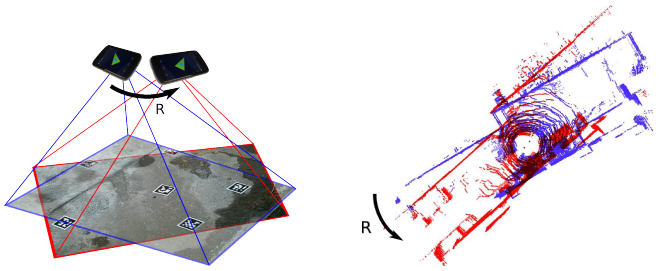

(a) Vision-based magnetometer calibration

(b) Laser-based magnetometer calibration

Fig. 1. Magnetometer calibration diagram: Proposed method to estimate the magnetometer's measurement bias using the relative rotation R obtained from the registration of two images or through laser scan-matching.

*This work was supported in part by the American Bureau of Shipping under award number N016970-UM-RCMOP.

G. Troni and R. Eustice are with the Department of Naval Architecture and Marine Engineering, University of Michigan, Ann Arbor, MI 48109, USA {gtroni, eustice}@umich.edu.

Kok et al. [12] make use of accelerometers to measure the local gravity vector to propose methods based on dot product corrections to estimate the magnetometer calibration. The drawback of these approaches is that translational accelerations of the instrument can perturb the measurements, introducing errors in the the magnetometer calibration.

Due to changes in the calibration parameters during operation, or the inability to estimate the calibration parameters before operation, many applications require the ability to perform the field sensor calibration continuously in real time. Crassidis and Lai [6] propose an extension to the TWOSTEP method based on an extended Kalman filter (EKF) and an unscented Kalman filter (UKF) to estimate in real time the sensor bias, scale, and orthogonality factors. Ma and Jiang proposed an alternative method based on an UKF [15] and Guo at al. [8] reported an EKF approach. These methods exhibit some of the same problems noted for the batch methods, and also do not ensure convergence of the estimated parameters to the true values. Recently, Troni and Whitcomb [26] proposed a method to estimate the magnetometer measurement bias aided by three-axis angular-rate gyroscopes. In constrast, our approach is based on angular *position* instead of angular *velocity* measurements, though it shares several of the same advantages of this previously reported method, such as: (*i*) it is empirically shown to be less restricted in the angular movements required, (*ii*) it does not require local field information, such as the magnitude and/or direction of the local magnetic field, (*iii*) it is implementable in real time, and (*iv*) it has convergence properties. In addition, our proposed method presents additional advantages such as: (1) our batch method does not require numerical differentiation of the magnetometer measurements, (2) it is independent of the sampling time between two compared measurements, making the proposed methods more suitable for systems with unreliable sources of time or low sampling rate, and (3) it is independent of the order of the measured signals, so it can use all the available information. The main disadvantage of the proposed approach, as compared to previous methods, is that calculating the relative rotation input, in case it is not available, might be a computationally expensive — but feasible even in real-time — process (e.g., image registration or laser scan-matching).

This paper is organized as follows. In Section II we give a brief overview of notation and describe the sensor error model. In Section III we describe our two proposed methods for sensor bias estimation. In Section IV we describe our experimental setup and we report a comparative numerical simulation and comparative experimental evaluation of the performance of the different sensor bias estimation methods. Section V summarizes and concludes.

II. Background

A. Mathematical Notation

We represent the rigid-body attitude using the rotation matrix $R(t) \in SO(3)$ describing the orientation of the instrument frame V with respect to an inertial (world) fixed frame W. The variable m_k is a discrete sample measurement (e.g., m_k represents a discrete-time sampling of $x(t_k)$ at time t_k). The Euclidean vector norm is defined as usual as $||x|| = (x^\top x)^{1/2}$, with $x \in \mathbb{R}^3$.

B. Sensor Error Model

Measurements from three-axis magnetometers are subject to systematic errors due to sensor bias, scale factor, and lack of orthogonality. We consider the usual bias model,

$$m_k = \bar{x}_k + b, \tag{1}$$

where $\bar{x}_k \in \mathbb{R}^3$ is the true field value in the instrument reference frame at t_k, $m_k \in \mathbb{R}^3$ is the measured field value in the instrument reference frame at t_k, and $b \in \mathbb{R}^3$ is an unknown constant sensor bias.

Three-axis magnetometers measure, in instrument coordinates, the Earth's local magnetic field, which is considered to be *locally* constant and fixed with respect to the inertial world-frame of reference. The true world-frame field vector m_0 is related to the instrument-frame sensor measurement of the field $\bar{x}_k$ by

$$m_0 = {}^{w}_{v}R_k \, (m_k - b), \tag{2}$$

where ${}^{w}_{v}R_k$ is the rotation matrix from the instrument frame to the world-frame at time t_k.

C. Visual Motion Estimation

The experiments considered here rely on visually-based motion estimation. Motion estimates from visual information can be extracted using different approaches. The methods can be categorized into direct (pixel-based methods, e.g., optical flow) [10], and indirect (feature-based methods) [25].

Referring to the pinhole camera model, a camera matrix is used to denote a projective mapping from world (3D), P_w, to pixel coordinates (2D), p_p, as follows

$$\begin{bmatrix} x_p \\ y_p \\ 1 \end{bmatrix} \propto K \begin{bmatrix} x_w \\ y_w \\ z_w \end{bmatrix}. \tag{3}$$

The camera intrinsics matrix K is defined as [9]

$$K = \begin{bmatrix} \alpha_x & s & c_x \\ 0 & \alpha_y & c_y \\ 0 & 0 & 1 \end{bmatrix}, \tag{4}$$

where (α_x, α_y) represent focal length in terms of pixels, (c_x, c_y) represent the principal point, and s represents the skew coefficient between the x and the y axis (often 0).

A relatively simple approach to estimate the relative camera motion is to use homography-based techniques [9]. A homography relates points in a plane, or for pure rotation motion between two camera views, as

$$p_2 = H \, p_1. \tag{5}$$

The relationship between the homography, H, with the relative camera motion (R, t) and the plane $\pi = [n, d]$ can be written as

$$H = K \, (R - t_n/d) \, K^{-1}. \tag{6}$$

For the case of very small camera translation, t, or large distance to the plane, d, H can be approximated with the infinity homography H_∞, as

$$H_\infty = K\ R\ K^{-1}. \tag{7}$$

From H_∞, we can calculate our relative camera rotation as

$$\tilde{R} = K^{-1}\ H_\infty\ K. \tag{8}$$

Due to small numerical inaccuracies, $\tilde{R}$ may not strictly lie within the family of SO(3) matrices so as final step we calculate R, the closest rotation matrix to $\tilde{R}$ under the Frobenius norm [18].

III. Proposed Methods

In this section we report a novel approach to estimate the 3-axis magnetometer measurement bias based on the relative rotation measurements (e.g., from a camera system). Two methods using this approach are proposed.

A. System Model

Taking two measurements from (2) yields

$$m_0 = {}^{w}_{v}R_j\ (m_j - b) = {}^{w}_{v}R_i\ (m_i - b), \tag{9}$$

where m_i and m_j are two measured magnetic field vectors in instrument coordinates at time t_i and t_j, respectively, and ${}^{w}_{v}R_i$ and ${}^{w}_{v}R_j$ are the corresponding rotation matrices from the instrument-frame to the world-frame. Defining ${}^{j}_{i}R = {}^{w}_{v}R_j^\top\ {}^{w}_{v}R_i$ yields

$$(m_j - b) = {}^{j}_{i}R\ (m_i - b), \tag{10}$$

and then rearranging the terms, we have

$$({}^{j}_{i}R - I)\ b = {}^{j}_{i}R\ m_i - m_j. \tag{11}$$

Note that the instrument absolute attitudes, ${}^{w}_{v}R_i$ and ${}^{w}_{v}R_j$, do not appear in (11), only the relative rotation between both measurements, ${}^{j}_{i}R$.

We wish to estimate the constant unknown sensor bias, b, for the system (11) from the signals m_i, m_j and ${}^{j}_{i}R$. The proposed solutions include (*i*) a batch least squares method and (*ii*) a real-time Kalman filter method.

B. Linear Least-Squares for Sensor Bias Calibration

Based on (11), the unknown sensor bias, b, can be estimated with linear least squares estimation. The sum of squared residuals cost function is

$$SSR(b) = \sum_{i=1}^{n-1} \sum_{j=i+1}^{n} \frac{1}{\sigma_{ij}^2} |({}^{j}_{i}R - I)\ b - {}^{j}_{i}R\ m_i + m_j|^2, \tag{12}$$

where σ_{ij} is the standard deviation of the measurements, and each measurement m_i is a discrete sample measurement at t_i. The linear least squares estimate for b is given by the well-known solution

$$\hat{b} = (\sum_{i=1}^{n-1} \sum_{j=i+1}^{n} \frac{1}{\sigma_{ij}^2} A_{ij}^\top A_{ij})^{-1} (\sum_{i=1}^{n-1} \sum_{j=i+1}^{n} \frac{1}{\sigma_{ij}^2} A_{ij}^\top\, y_{ij}), \tag{13}$$

where $A_{ij} \in \mathbb{R}^{3\times 3}$ is the calculated matrix $A_{ij} = {}^{j}_{i}R - I$, and $y_i \in \mathbb{R}^3$ is the calculated vector from the measurements, $y_i = {}^{j}_{i}R\ m_i - m_j$. The solution (13) uniquely exists when the set axis of rotation vectors, $\{\omega_{ij}\} \in \mathbb{R}^3$, of the set of rotation matrices, ${}^{j}_{i}R$, are not all collinear, in consequence, $\sum_{i=1}^{n-1} \sum_{j=i+1}^{n} \frac{1}{\sigma_{ij}^2} A_{ij}^\top A_{ij}$ is invertible.

The proposed method is flexible. For example, it can be implemented based on information from matching all images against each other, only consecutive images or each image against a selected key frame image.

C. Kalman Filter for Sensor Bias Calibration

To implement a real-time Kalman filter method, the system (11) can be rewritten as

$$\underbrace{\begin{bmatrix} m_k \\ b \end{bmatrix}}_{\Phi_k} = \underbrace{\begin{bmatrix} {}^{k}_{k\text{-}1}R & I - {}^{k}_{k\text{-}1}R \\ 0 & I \end{bmatrix}}_{A_k} \underbrace{\begin{bmatrix} m_{k\text{-}1} \\ b \end{bmatrix}}_{\Phi_{k\text{-}1}}, \tag{14}$$

with the measurement model

$$z_k = \underbrace{[I \quad 0]}_{H} \begin{bmatrix} m_k \\ b \end{bmatrix}, \tag{15}$$

and we can define the following discrete linear time-varying system

$$\begin{aligned} \Phi_k &= A_k\ \Phi_{k\text{-}1} + \nu_1(t), \quad \nu_1(t) \sim \mathcal{N}(0, Q), \\ z_k &= H\Phi_k + \nu_2(t), \qquad \nu_2(t) \sim \mathcal{N}(0, R). \end{aligned} \tag{16}$$

The sensor bias estimate can be solved with a standard discrete-time Kalman filtering implementation [4], [11].

The sufficient conditions for observability of the linear time-varying (LTV) system (16) can be shown by a rank test (see [24], Theorem 25.9),

$$rank \underbrace{\begin{bmatrix} I & 0 \\ {}^{k}_{k\text{-}1}R & I - {}^{k}_{k\text{-}1}R \\ {}^{k+1}_{k}R\,{}^{k}_{k\text{-}1}R & I - {}^{k+1}_{k}R\,{}^{k}_{k\text{-}1}R \end{bmatrix}}_{\Theta} = 6. \tag{17}$$

Note that for full column rank of the matrix Θ, the equation $\Theta z \neq 0$ should hold for all $z \neq 0$. If $z = [z_1\ z_2]^\top$, then it is required that $z_2 - {}^{k}_{k\text{-}1}R\, z_2 \neq 0$ or $z_2 - {}^{k+1}_{k}R^{k}_{k\text{-}1}R\, z_2 \neq 0$ for any $z_2 \neq 0$. That is equivalent to ${}^{k}_{k\text{-}1}R\, z_2 \neq z_2$ or ${}^{k+1}_{k}R\, z_2 \neq z_2$ for any $z_2 \neq 0$. Then a sufficient condition for system (16) is observable on $[t_0, t_f]$ if for some $t_k, t_{k+1} \in [t_0, t_f]$, the axis of two sampled rotation matrices ${}^{k}_{k\text{-}1}R$ and ${}^{k+1}_{k}R$ are not collinear.

IV. Performance Evaluation

We compared the performance of the following five methods for the problem of sensor bias estimation. Three batch estimation methods were evaluated:

a. ***Centering***: For comparison purposes, the sensor bias is estimated using the first step of the TWOSTEP method [3] that leads to a simple batch linear least squares solution.
b. ***TWOSTEP***: For comparison purposes, the sensor bias is estimated using the TWOSTEP method [3].

c. ***VMC-LS***: The sensor bias is estimated using the batch method proposed in Section III-B based on relative rotation motion in the instrument-frame. The measurements are low-pass filtered and re-sampled at the camera frame rate.

In addition, two real-time methods were evaluated:

d. ***AI-EKF***: For comparison purposes, the sensor bias is estimated using the real-time attitude independent method based on the EKF [6]. Note that for an accurate comparison the implemented version of this method only estimates the sensor bias, and not the scale and orthogonality matrix.

e. ***VMC-KF***: The sensor bias is estimated using the Kalman filter method described in Section III-C based on relative rotation motion in the instrument-frame.

For comparing the real-time estimation methods (AI-EKF and VMC-KF), the sensor measurement bias used for comparing with the batch methods consists of the average of the last 50% of the estimated sensor measurement bias. The TWOSTEP and AI-EKF methods require knowledge of the local magnetic field magnitude. In our evaluation we used the standard US/UK World Magnetic Model for 2010–2015 [16] available online [1]. For comparison purposes we also evaluate the case of running the TWOSTEP method with a manually selected value of local magnetic field magnitude estimated *in-situ* before each experiment in order to improve the performance of this method (instead of using the less accurate value from models for our case). We denote this case as TWOSTEP*. The camera alignment to the inertial measurement unit was manually measured and compensated in the experimental evaluation.

A. Simulation Results

A Monte Carlo simulation was implemented with 1000 trials for two different types of datasets. The first dataset, SIM1L, simulates the case of large angular movements of the instrument in all degrees of freedom, as depicted in Fig. 2(a). The second dataset, SIM2S, simulates a constrained angular movement of the instrument, as depicted in Fig. 2(b). The duration of each experiment is 120 s and the simulated sensor data is generated at 4 Hz. Gaussian noise was added to the simulated magnetometer measurements ($\sigma_{mag} = 1$ mG), and the simulated relative rotation measurements ($\sigma_R = 1°$). The true magnetic field vector is $x_0 = [200,\ -40,\ 480]^\top$ mG and the bias is $b = [20,\ 120,\ 90]^\top$ mG. The magnitude of the magnetic field used for the TWOSTEP and AI-EKF methods was 1% greater than the value used in generating the simulated data. The covariance matrices used by the AI-EKF and VMC-KF methods are $Q = 0.1\mathrm{I}_{6\times6}$ mG and $R = \mathrm{I}_{3\times3}$ mG. These values were chosen in the range of the expected process and sensor noises. Fig. 3 shows the estimation performance for each simulated experiment.

The simulation results show that for a complete range of movements (i.e., SIM1L), the batch methods Centered, TWOSTEP, and VMC-LS show the best performance with an average error under 0.2 mG for the magnetometer bias estimate. The VMC-KF method shows good estimation performance of the magnetometer bias with an error under 0.5 mG. The worst performance is shown by the AI-EKF method with bias estimation errors over 5 mG. The AI-EKF method is affected by linearization errors and does not ensure convergence. For the second dataset, SIM2S, the proposed methods, VMC-LS and VMC-KF, show the best performance, with bias estimation errors under 2–3 mG.

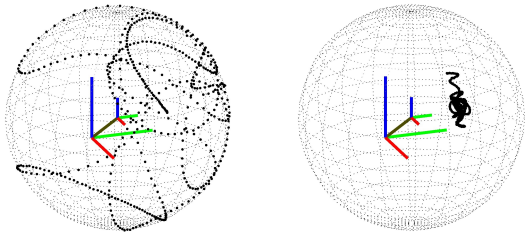

(a) Sim. data SIM1L: Large movements

(b) Sim. data SIM2S: Constrained movements

Fig. 2. Simulated magnetometer data: Three-dimensional plot of the simulated magnetometer data (black dots). For reference, a sphere is plotted centered at *b*. The large reference-frame is at (0,0,0) with x-axis in red, y-axis in green, and z-axis in blue. A small reference-frame is plotted at the center of the sphere. The line connecting the large and small reference-frames represent the sensor measurement bias.

The other methods (Centered, TWOSTEP, and AI-EKF) show a bias estimation error over 10 mG. Note that the TWOSTEP and AI-EKF methods are very sensitive to errors in the used value of the *a priori* magnitude of the local magnetic field. For small movement experiments (such as SIM2S), we notice that the sensor bias estimation error grows proportionally to the error in the magnitude of the magnetic field. In our simulation performance evaluation, an error in the magnitude used for estimation is introduced representing 1% of the real magnitude. But for common applications, the difference between the local magnitude of the magnetic field and that predicted by the model can include much higher errors (such as inside/near buildings or other unknown magnetic anomalies).

These simulation results support the utility of all proposed methods. In the next section we evaluate the performance for experimental data.

B. Experimental Results

This section reports the results of a comparative experimental performance evaluation of the five calibration methods in experimental trials of systems equipped with a micro-electro-mechanical systems (MEMS) magnetometers and a camera. For our experimental performance evaluation we use two different experimental setups: an indoor laboratory experimental setup and an outdoor phone-based experimental setup. The experimental setups are depicted in Fig. 4.

1) **Indoor laboratory experimental setup**: For measuring the magnetic field we use a MEMS-based attitude and heading reference system (AHRS), the Microstrain 3DM-GX3-25 [17]. Images were captured with a Point Grey Chameleon camera with a resolution of 1280 by 960

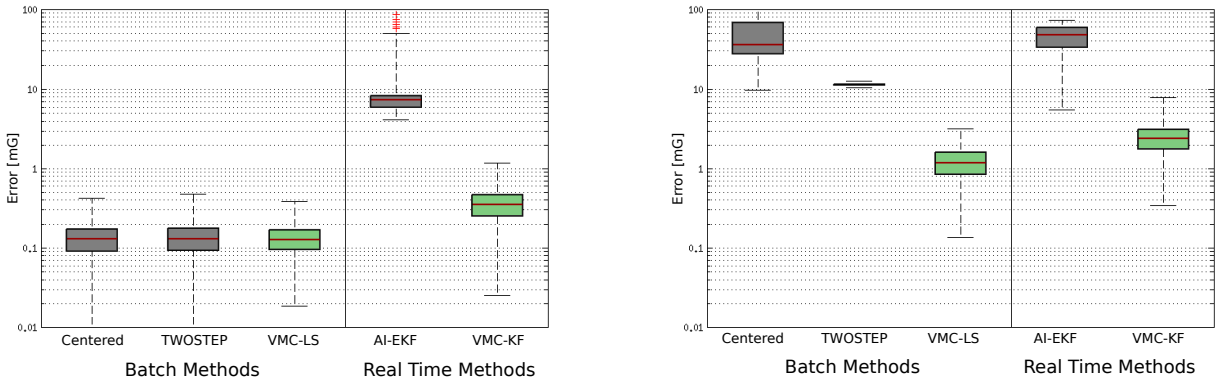

(a) Simulation results from SIM1L: Large angular movements

(b) Simulation results from SIM2S: Constrained angular movements

Fig. 3. Performance evaluation results from simulated data: The y-axis shows the sensor bias estimation error for each solution (mG) in logarithmic scale. Each box plot is calculated from 1000 trials. The proposed methods' (VMC-LS and VMC-KF) estimation performance is less sensitive with constrained angular movements while previously reported methods' (Centered, TWOSTEP, AI-EKF) estimation performance is significantly reduced.

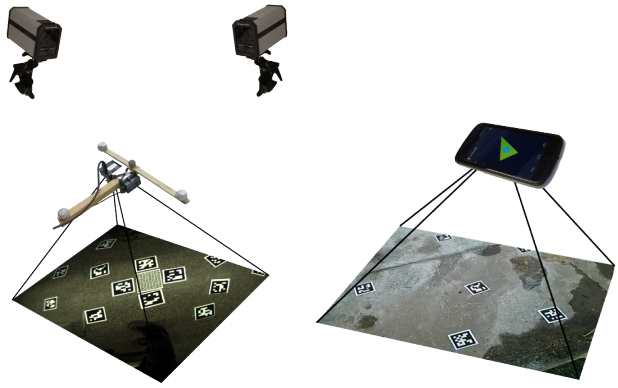

(a) Laboratory experimental setup (b) Phone experimental setup

Fig. 4. Experimental setups.

pixels [22]. Data was recorded at 4 Hz. For comparing the heading estimation performance, we used the Qualisys ProReflex motion capture system MCU 1000 [23] as "ground-truth" heading.

2) **Outdoor phone experimental setup**: We use a LG Nexus 4 mobile phone with a three-axis accelerometer, three-axis gyroscope, and three-axis magnetometer included. The images from the back camera were acquired at 640 by 480 pixels. Data was recorded at 3.5 Hz. For comparing the heading estimation performance, we used the estimated relative attitude to visual markers in the scene (AprilTags [21]) to compute our "ground-truth" heading.

We computed the relative rotation inputs using the OpenCV library [5] following a commonly used visual odometry pipeline:

1) Image acquisition: We acquired and time stamped the images at $3.5 - 4.0$ fps.
2) Feature detection: SIFT features and descriptors [14] are detected in grayscale calibrated images.
3) Matching: Features from two correlative images are matched using the randomized kd-tree forest implemented in the FLANN (Fast Approximate Nearest Neighbor Search) library [19].
4) Homography: Homography is calculated with outlier rejection using Random Sample Consensus (RANSAC), [9].
5) Motion estimation: We calculate the relative rotation estimate from (8).

It should be noted that although the AprilTag markers were present in both experiments, we did not use them to improve the visual motion estimate previously described. In practice, the number of features introduced for the AprilTags markers was significantly smaller than the features detected on the background.

Four experiments were performed. Two experiments in the laboratory facility, EXP1L and EXP2S, and two experiments outside with a mobile phone, EXP3L and EXP4S. The first experiment for each setup, EXP1L and EXP3L, measure a large range of movements, Fig. 5(a) and 5(c). The trajectory is a sequence of large heading, pitch, and roll rotations. Most of these trajectories are not feasible to implement in many robotic vehicles. The second experiment for each setup, EXP2S and EXP4S, measures a more feasible sequence of movements, Fig. 5(b) and 5(d), where the range of movement of the system is limited in heading, pitch, and roll. The data was collected and bias estimation executed and analyzed off-line.

For our analysis, the estimation is performed for all the evaluated methods using raw measurements from the sensor including the measured orthogonality and scale factor distortions. The unaccounted error in the scale factor can show the robustness to perturbations of the proposed methods that are not compensating for these errors. In practice, the orthogonality scale factor matrix can be measured previously and compensated to improve the performance of the system, to later use the proposed methods to continue estimating the sensor bias under different conditions.

TABLE I

SUMMARY OF THE SENSOR BIAS ESTIMATION RESULTS FROM LABORATORY EXPERIMENTS (EXP1L AND EXP2S) AND PHONE EXPERIMENTS (EXP3L AND EXP4S). BEST HEADING ESTIMATION PERFORMANCE IN EACH EXPERIMENT IS MARKED IN BOLD FONT.

	EXP1L - LABORATORY				EXP2S - LABORATORY				EXP3L - PHONE				EXP4S - PHONE			
	$\hat{b}_x$ [mG]	$\hat{b}_y$ [mG]	$\hat{b}_z$ [mG]	$\sigma(h_E)$ [deg]	$\hat{b}_x$ [mG]	$\hat{b}_y$ [mG]	$\hat{b}_z$ [mG]	$\sigma(h_E)$ [deg]	$\hat{b}_x$ [mG]	$\hat{b}_y$ [mG]	$\hat{b}_z$ [mG]	$\sigma(h_E)$ [deg]	$\hat{b}_x$ [mG]	$\hat{b}_y$ [mG]	$\hat{b}_z$ [mG]	$\sigma(h_E)$ [deg]
Raw	-0.0	-0.0	-0.0	8.5	-0.0	-0.0	-0.0	8.5	0.0	0.0	-0.0	100.5	0.0	0.0	-0.0	100.5
Centered [7]	-35.1	-45.3	-59.7	3.1	-11.5	-61.7	-61.2	4.0	67.0	801.5	-622.0	4.2	79.8	760.8	-584.8	6.0
TWOSTEP [3]	-34.8	-43.2	-59.8	3.1	26.0	32.5	-57.6	8.0	67.7	817.6	-713.4	6.2	12.7	949.5	-762.5	28.4
TWOSTEP* [3]	-35.1	-45.0	-59.7	3.1	-4.2	-43.4	-60.5	4.3	67.1	802.8	-629.1	4.3	59.9	817.2	-637.9	5.3
VMC-LS	-24.6	-33.7	-49.7	**2.5**	-17.0	-33.2	-49.5	**2.8**	85.7	800.3	-597.8	4.2	86.6	789.4	-603.8	4.5
AI-EKF [6]	-20.2	62.8	-63.0	6.2	26.6	39.6	-56.7	8.2	228.2	427.9	194.5	206.8	192.3	102.5	24.7	111.8
VMC-KF	-30.3	-43.1	-43.1	2.7	-11.7	-30.9	-41.1	3.4	84.6	804.3	-599.7	**4.2**	87.4	795.5	-592.6	**4.3**

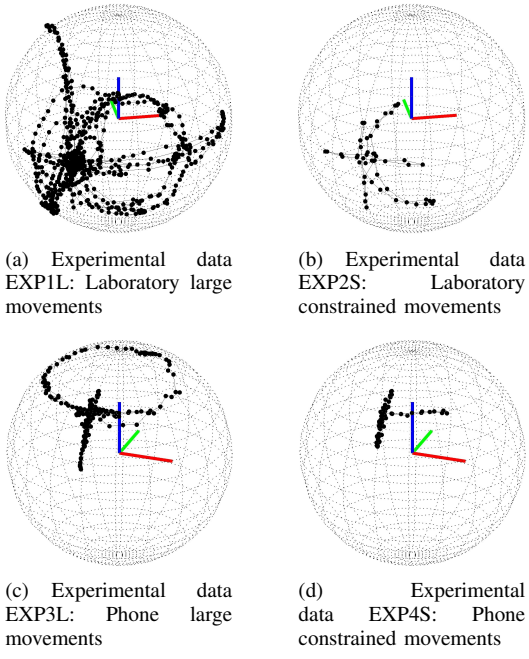

(a) Experimental data EXP1L: Laboratory large movements

(b) Experimental data EXP2S: Laboratory constrained movements

(c) Experimental data EXP3L: Phone large movements

(d) Experimental data EXP4S: Phone constrained movements

Fig. 5. Experimental evaluation data: Three-dimensional plot of the magnetometers' recorded data for each experiment (black dots). For reference, a sphere is plotted centered at the best estimate of the sensor measurement bias. A reference-frame is plot at the center of the sphere with x-axis in red, y-axis in green, and z-axis in blue.

Magnetometer bias was estimated with each evaluated method using data from EXP1L to EXP4S. From each estimated magnetometer bias, $\hat{b}_q$, we calculate the heading error, h_{Eq}, between the heading, h_q, calculated from the magnetometer data with the estimated bias $\hat{b}_q$ removed, and the heading from the visual tags, h_{REF}. For a more accurate heading comparison in the case of the constrained experiments, EXP2S and EXP4S, we use the same data, from EXP1L and EXP3L, respectively, to calculate the heading error. Table I summarizes the experimental results.

From the performance evaluation in Table I, the VMC-LS and VMC-KF methods show good performance in all four experiments, correcting the heading error from the original 8.5–100° range to less than 3° for laboratory experiments and 4.5° for phone experiments. On the other hand, the Centered and TWOSTEP methods only show good performance for the large angular movement experiments, EXP1L and EXP3L, but they are less accurate for a more limited calibration dataset, EXP2S and EXP3S. For EXP2S, the Centered and TWOSTEP methods show error increase in 1–20° from the original error with EXP1L. For the case of the manually selected magnetic field magnitude for each experiment, TWOSTEP*, the results are better than TWOSTEP in all cases but not as good as the proposed methods VMC-LS and VMC-KF for the constrained angular movement experiments, EXP2S and EXP4S. AI-EKF, like in the numerical simulations, shows worst performance of the evaluated methods, and it is not able to estimate the bias and improve the heading estimate for the phone experiments EXP3L and EXP4S. This is due to the large initial bias for the phone increasing the linearization errors of the EKF, making the filter to not converge to the correct estimate of the bias.

Fig. 6 shows the sensor bias estimate over time for the two real time evaluated methods (AI-EKF and VMC-KF) for EXP3L and EXP4S. The results show that the bias is correctly estimated only for VMC-KF but not for AI-EKF. The VMC-KF method converges in less than 18 s (EXP3L) and 12 s (EXP4S). The b_x and b_y values converge fastest due to the nature of the excitation with large heading movements.

V. CONCLUSIONS

The proposed relative angular position aided estimation methods (VMC-LS and VMC-KF) were shown to improve the sensor bias estimation performance under some circumstances with limited range of movement of the system when compared with the previously reported methods (Centered, TWOSTEP, and AI-EKF).

The numerical simulation and experimental results quantified the sensor measurement bias estimation performance under different scenarios of calibration motions. The proposed methods, VMC-LS and VMC-KF, show good performance for all the evaluated scenarios. The previously reported methods, Centered, TWOSTEP, and AI-EKF, show good performance only when the data contains large angular motion. In addition, TWOSTEP and AI-EKF methods require exact knowledge of the magnitude of the local magnetic field vector, and are very sensitive to error in this value.

The comparative experimental evaluation quantified the resulting calibrated heading estimation performance when

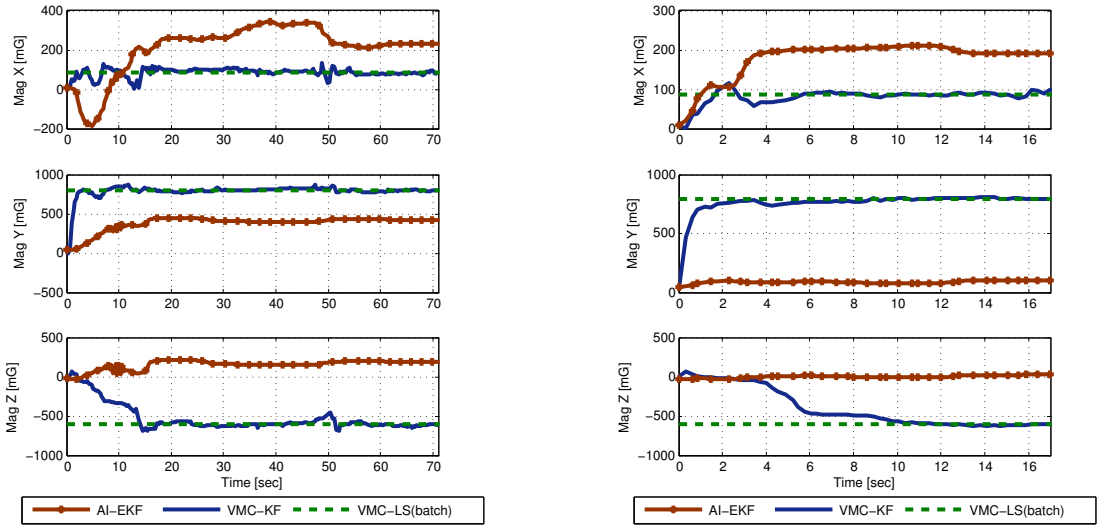

(a) Magnetometer bias estimation over time for EXP3L

(b) Magnetometer bias estimation over time for EXP4S

Fig. 6. The x-axis shows the time (seconds) and the y-axis the estimated bias for each method (mG). The AI-EKF method is shown in dotted red and the VMC-KF method in solid blue. As a reference, the offline bias estimated by the VMC-LS method is shown as dashed green.

compared with the heading estimated by a motion capture system and visual markers outside. The proposed method, VMC-LS and VMC-KF, show significantly smaller heading error after calibration than all the previously reported methods for the case of a more feasible sequence of calibration movements for most ground, marine, or aerial vehicles. Finally, the proposed real-time method, VMC-KF, ensures convergence to the estimated sensor bias value while the previously proposed method, AI-EKF, does not ensure convergence to the true values.

REFERENCES

[1] The world magnetic model. National oceanic and atmospheric administration (NOAA). `http://www.ngdc.noaa.gov/geomag/WMM/DoDWMM.shtml`.

[2] R. Alonso and M. D. Shuster. Complete linear attitude-independent magnetometer calibration. *J. Astronautical Sciences*, 50(4):477–490, 2002.

[3] R. Alonso and M. D. Shuster. TWOSTEP, a fast robust algorithm for attitude-independent magnetometer bias determination. *J. Astronautical Sciences*, 50(4):433–451, 2002.

[4] Y. Bar-Shalom, T. Kirubarajan, and X.-R. Li. *Estimation with Applications to Tracking and Navigation*. John Wiley & Sons, Inc., New York, NY, USA, 2001.

[5] G. Bradski and A. Kaehler. *Learning OpenCV: Computer vision with the OpenCV library*. O'Reilly, 2008.

[6] J. L. Crassidis, K. L. Lai, and R. R. Harman. Real-time attitude-independent three-axis magnetometer calibration. *J. Guidance Control and Dynamics*, 28(1):115–120, 2005.

[7] B. Gambhir. Determination of magnetometer biases using module RESIDG. Computer Sciences Corporation, Report No.3000-32700-01TN. Technical report, Mar. 1975.

[8] P. Guo, H. Qiu, Y. Yang, and Z. Ren. The soft iron and hard iron calibration method using extended kalman filter for attitude and heading reference system. In *IEEE/ION Pos., Loc. and Nav. Symp.*, pages 1167–1174, Monterey, CA, May 2008.

[9] R. I. Hartley and A. Zisserman. *Multiple View Geometry in Computer Vision*. Cambridge University Press, 2nd edition, 2004.

[10] M. Irani and P. Anandan. All about direct methods. In W. Triggs, A. Zisserman, and R. Szeliski, editors, *Int. Workshop on Vis. Alg.*, pages 278–295, 1999.

[11] R. Kalman. A new approach to linear filtering and prediction problems. *J. Basic Engineering*, 82(1):35–45, 1960.

[12] M. Kok, J. D. Hol, T. B. Schon, F. Gustafsson, and H. Luinge. Calibration of a magnetometer in combination with inertial sensors. In *Int. Conf. Information Fusion*, pages 787–793, Singapore, July 2012.

[13] X. Li and Z. Li. A new calibration method for tri-axial field sensors in strap-down navigation systems. *Measurement Science and Technology*, 23(10):105105, 2012.

[14] D. G. Lowe. Distinctive image features from scale-invariant keypoints. *Int. J. Comput. Vis.*, 60(2):91–110, 2004.

[15] G.-F. Ma and X.-Y. Jiang. Unscented kalman filter for spacecraft attitude estimation and calibration using magnetometer measurements. In *Proc. Int. Conf. Machine Learning and Cybernetics*, pages 506–511, Guangzhou, China, Aug. 2005.

[16] S. Maus, S. Macmillan, S. McLean, B. Hamilton, A. Thomson, M. Nair, and C. Rollins. The US/UK World Magnetic Model for 2010-2015. Technical report, Dec. 2010.

[17] Microstrain Inc. *3DM-GX3-25 Miniature Attitude Heading Reference System datasheet.* Williston, VT, 2012.

[18] M. Moakher. Means and averaging in the group of rotations. *SIAM J. Matrix Analysis and App.*, 24(1):1–16, 2002.

[19] M. Muja and D. G. Lowe. Fast approximate nearest neighbors with automatic algorithm configuration. In *Int. Conf. Computer Vis. Theory and App.)*, pages 331–340, 2009.

[20] D. Nistér, O. Naroditsky, and J. Bergen. Visual odometry. In *Proc. IEEE Conf. Comput. Vis. Pattern Recog.*, pages 652–659 Vol.1, Washington, DC, June 2004.

[21] E. Olson. AprilTag: A robust and flexible visual fiducial system. In *Proc. IEEE Int. Conf. Robot. and Automation*, pages 3400–3407, Shanghai, China, May 2011.

[22] Point Grey Research Inc. *Chameleon Technical Reference Manual*. Richmond BC, Canada, 1.6 edition, 2011.

[23] Qualisys AB. *QualisysTrack Manager, user manual.* Gothenburg, Sweden, 2011.

[24] W. Rugh. *Linear Systems Theory*. Prentice Hall PTR, 2nd edition, 1996.

[25] P. H. S. Torr and A. Zisserman. Feature based methods for structure and motion estimation. In W. Triggs, A. Zisserman, and R. Szeliski, editors, *Int. Workshop on Vis. Algorithms*, pages 278–295, 1999.

[26] G. Troni and L. Whitcomb. Adaptive estimation of measurement bias in three-dimensional field sensors with angular rate sensors: Theory and comparative experimental evaluation. In *Proc. Robot.: Sci. & Syst. Conf.*, Berlin, Germany, June 2013.

[27] J. F. Vasconcelos, G. Elkaim, C. Silvestre, P. Oliveira, and B. Cardeira. Geometric approach to strapdown magnetometer calibration in sensor frame. *IEEE Trans. Aerosp. Electron. Syst.*, 47(2):1293–1306, 2011.